Functional imaging of murine hearts using accelerated self-gated UTE cine MRI

Int J Cardiovasc Imaging (2015) 31:83–94
DOI 10.1007/s10554-014-0531-8

ORIGINAL PAPER

Functional imaging of murine hearts using accelerated self-gated UTE cine MRI

Abdallah G. Motaal · Nils Noorman · Wolter L. de Graaf · Verena Hoerr · Luc M. J. Florack · Klaas Nicolay · Gustav J. Strijkers

Received: 9 July 2014 / Accepted: 2 September 2014 / Published online: 10 September 2014

Abstract We introduce a fast protocol for ultra-short echo time (UTE) Cine magnetic resonance imaging (MRI) of the beating murine heart. The sequence involves a self-gated UTE with golden-angle radial acquisition and compressed sensing reconstruction. The self-gated acquisition is performed asynchronously with the heartbeat, resulting in a randomly undersampled k*t*-space that facilitates compressed sensing reconstruction. The sequence was tested in 4 healthy rats and 4 rats with chronic myocardial infarction, approximately 2 months after surgery. As a control, a non-accelerated self-gated multi-slice FLASH sequence with an echo time (TE) of 2.76 ms, 4.5 signal averages, a matrix of 192 × 192, and an acquisition time of 2 min 34 s per slice was used to obtain Cine MRI with 15 frames per heartbeat. Non-accelerated UTE MRI was performed with TE = 0.29 ms, a reconstruction matrix of 192 × 192, and an acquisition time of 3 min 47 s per slice for 3.5 averages. Accelerated imaging with 2×, 4× and 5× undersampled k*t*-space data was performed with 1 min, 30 and 15 s acquisitions, respectively. UTE Cine images up to 5× undersampled k*t*-space data could be successfully reconstructed using a compressed sensing algorithm. In contrast to the FLASH Cine images, flow artifacts in the UTE images were nearly absent due to the short echo time, simplifying segmentation of the left ventricular (LV) lumen. LV functional parameters derived from the control and the accelerated Cine movies were statistically identical.

Keywords Compressed sensing · UTE · Cardiac MRI · Functional imaging

Electronic supplementary material The online version of this article (doi:10.1007/s10554-014-0531-8) contains supplementary material, which is available to authorized users.

A. G. Motaal (✉) · N. Noorman · W. L. de Graaf · K. Nicolay · G. J. Strijkers
Biomedical NMR, Department of Biomedical Engineering, Eindhoven University of Technology, Eindhoven, The Netherlands
e-mail: a.motaal@tue.nl

A. G. Motaal · N. Noorman · W. L. de Graaf · K. Nicolay · G. J. Strijkers
Center for Imaging Research and Education (CIRE), Eindhoven, The Netherlands

A. G. Motaal · L. M. J. Florack
Department of Mathematics and Computer Science, Eindhoven University of Technology, Eindhoven, The Netherlands

V. Hoerr
Department of Clinical Radiology, University Hospital of Münster, Münster, Germany

G. J. Strijkers
Department of Biomedical Engineering and Physics, Academic Medical Center, Amsterdam, The Netherlands

Introduction

Cardiovascular magnetic resonance imaging (MRI) is considered the gold standard for accurate assessment of cardiac anatomy and function [1–3]. In murine animal models of myocardial diseases MRI provides a unique technique to get detailed longitudinal information on disease progression [4, 5]. Nevertheless, there are considerable experimental limitations to the small animal cardiovascular MRI. The small size of the murine heart requires high imaging gradients that may lead to ECG distortions and unreliable cardiac and respiratory triggering. The high heart rate and high blood flow velocities result in residual movement artifacts in the images.

Moreover, full heart coverage requires lengthy acquisitions [6–8].

Signal voids and ghosting due to rapid blood flow are the most pronounced artifacts in the standard FLASH Cine MRI acquisition of the murine heart. Additionally, susceptibility artifacts near the lungs and liver may result in signal loss. Both types of artifacts can be mitigated by decreasing the echo time (TE). However, in the FLASH sequence TE cannot be chosen adequately short due to image resolution requirements and bandwidth limitations [9].

A solution to flow and susceptibility related artifacts can be found in the use of an ultra-short echo time (UTE) sequence [10, 11]. The use of a radial readout shortens TE considerably and enables artifact-free Cine of the murine heart, as was shown previously by Hoerr et al. [12]. In the latter study a self-gating technique was used for cardiac triggering and respiratory gating. Heart and respiratory movements were obtained from the center k-space point that is acquired every TR in the radial readout scheme. Movies were reconstructed by retrospectively binning data into the desired cardiac time frames [13–16]. Drawbacks of this retrospective gating scheme is the long acquisition time that is needed to ensure full stochastic filling of k-space for each cardiac time frame, as each k-line has to be measured at least once. Assignment of echoes to the different k-space time points is a random process that depends on the asynchronous timing of TR with respect to heart and respiration rates [15]. Moreover, to fulfill the radial Nyquist criterion more k-spokes, readouts, need to be measured than for an equal image matrix in regular Cartesian FLASH imaging, leading to an even longer imaging time. To reduce the acquisition time, novel sparse sampling and reconstruction strategies such as compressed sensing (CS) can be employed. The radial readout scheme of the UTE sequence fits very well with the CS requirements and high acceleration factors can be achieved [17].

In this paper, we introduce a fast protocol for multi-slice Cine MRI of the murine heart, which combines a self-gated radial UTE Cine sequence and CS reconstruction, where a golden-angle undersampling scheme is used to provide homogenous coverage and higher incoherence of the undersampling artifacts. The sequence was tested in 4 healthy rats and 4 rats with chronic myocardial infarction, approximately 2 months after surgery. The technique was validated in a comparison to regular non-accelerated self-gated multi-slice FLASH sequence.

Materials and methods

MRI protocol and In vivo measurements

Scanning was performed with a 7T Bruker animal scanner (Bruker BioSpin MRI GmbH, Ettlingen, Germany). The gradient system allowed a maximal gradient strength of 660 mT/m with a slew rate of 4570 T/m/s. A 86 mm quadrature coil (Bruker BioSpin) was used for RF transmission and a 4 × 1 cardiac phased array coil (Bruker BioSpin) was used for RF reception. To determine the orientation of the short axis, several scout images were acquired in the transverse plane and the long-axis plane of the left ventricle at the start of each examination.

The local institutional animal care committee (Maastricht University, Maastricht, The Netherlands) reviewed and approved all experimental procedures. In this study, 8 male Lewis rats (Charles River, Paris, France) 12 weeks of age were used. All animals underwent surgery, where in 4 rats ligation of the left anterior descending artery (LAD) was performed to induce chronic myocardial infarction, while for the other 4 rats no knot was placed and/or pulled in the ligation suture. During surgery animals were anesthetized using inhalation anesthesia (2–3 % Isoflurane in oxygen (0.8 l/min) after intubation). Animals were placed on a heating pad and their temperature was checked by a rectal probe and maintained between 36 and 37.5 °C. To treat pain, sufentanil as an analgesic was used during the procedure, and after recovery buprenorphine was given subcutaneously up to at least 48 h. Animals were daily checked for weight, hydration, behavior, pain and wound healing. No animals died during or directly after the ligation procedure. Animals were housed under specific pathogen free (SPF) conditions with two per cage and were provided with food and water ad libitum. The imaging experiments were performed 2 months after the surgery. During imaging, rats were sedated by inhalation of 2–3 % isoflurane in oxygen (0.8 l/min). Temperature was maintained at 36–37.5 °C with a heating pad and monitored using a rectal probe.

As a reference, a standard multi-slice short axis self-gated FLASH sequence was used with 5 slices (NS = 5) covering the heart from base to apex. Self-gating was performed using an in-slice navigator echo. Sequence parameters were: Gaussian-shaped RF pulse of 300 μs; flip angle = 15°; TR = 8 ms; TE = 2.76 ms; field of view = 5 × 5 cm^2; acquisition matrix (NF × NP) = 192 × 192; reconstruction matrix = 256 × 256; slice thickness = 1 mm; number of repetitions (NR) per slice = 100. This number of repetitions resulted in number of averages NA = 4.5 ± 0.3 on average over the 8 animals. The resulting total acquisition time was NR × NP × TR ≈ 2 min 34 s per slice. Cine movies with 15 frames per slice were reconstructed retrospectively.

For the proposed method, a multi-slice self-gated 2D UTE sequence was implemented as schematically shown in Fig. 1a. Imaging was performed in the same geometry (short axis) and with the same number of slices (NS = 5) as for the reference datasets. Sequence parameters were:

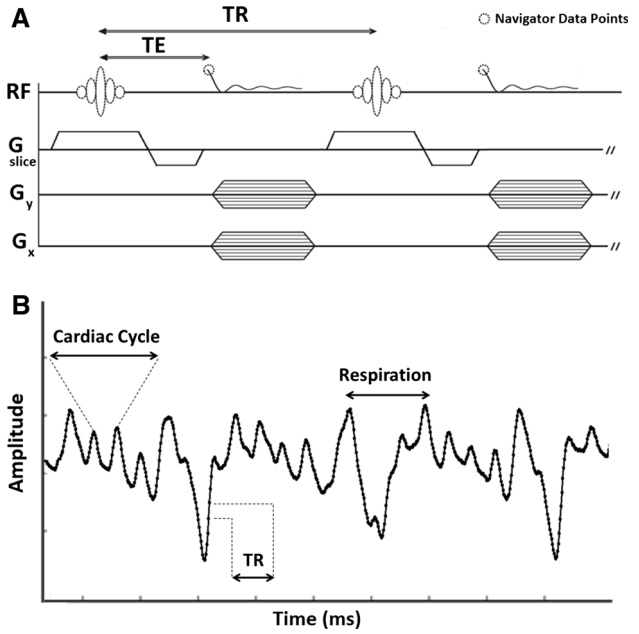

Fig. 1 Schematic of the 2D self-gated UTE sequence. **a** Readout is performed with short TE and directly after the slice-refocusing gradient. A navigator signal for the recording of cardiac and respiratory motion is extracted from the first point (*circle*) of the readout. **b** Representative example of a navigator signal trace as function of time. The rapid oscillation in the amplitude is due to cardiac motion, whereas the larger changes in amplitude are due to respiration. The *solid line* is a spline fit through the individual navigator samples (*solid circles*)

Gaussian-shaped RF pulse of 300 μs; flip angle = 15°; TR = 5 ms; TE = 0.29 ms; field of view = 5 × 5 cm^2; readout data (Number Radial Spokes (NP) × Spoke Length) = 604 × 96; reconstruction matrix = 256 × 256; slice thickness = 1 mm; number of repetitions (NR) = 75 resulting in NA = 3.4 ± 0.2 on average over the eight animals. The resulting total acquisition time was NP × TR × NR ≈ 3 min 47 s min per slice. The radial spokes that were sampled with golden-angle angular spacing, have been assigned to the corresponding time frames and Cine images have been reconstructed using a non-uniform fast Fourier transform (NUFFT) [18].

The navigator echo analyses were done retrospectively with homebuilt software in Matlab 8.1 using a local maximum detection algorithm to determine the start of the cardiac cycle. K-spokes acquired during respiration (~30 % of the data) were discarded. Unless stated otherwise, Cine movies were reconstructed with 15 cardiac time frames.

Shorter acquisition times were achieved by taking the first 1 min, 30, and 15 s of the fully sampled data that correspond to approximately 2×, 4×, and 5× undersampled k-space data, respectively. The % k-space filling and effective number of averages varied over the animals and cardiac time frames because of the stochastic filling method. In Table 1 the different protocols are listed with the acquisition time per slice, as well as the effective k-space filling percentages and NA averaged over the 8 animals.

CS reconstruction

Compressed sensing (CS) has proven a valuable technique for speeding up data acquisition in MRI by exploiting the compressibility of MR images [19–22]. The ability to transform the data to a sparse representation and the radial trajectory, which is used in Cine UTE imaging, fits very well with the sparsity and incoherence requirements for CS.

Due to the stochastic nature of the retrospective gating acquisition, a randomly undersampled k*t*-space was achieved. The resulting k*t*-space, sampled at significant sub-Nyquist rates, was reconstructed with a non-linear compressed sensing algorithm. Mathematically, the following constrained optimization problem was solved:

$$\min||\psi(\mathrm{m})||_1 \; subject\; to\; ||\mathrm{R}^{-1}\mathrm{F_s m}-\mathrm{y}||_2 < \varepsilon, \qquad (1)$$

where ψ is the sparsifying transformation, m is the reconstructed data, y is the measured undersampled k*t*-space, and F_s is the sampled Fourier transformation and R is a gridding operator that interpolates the Fourier data to radial spokes to ensure data consistency with acquired data, and ε controls the fidelity of the reconstructed to the measured data. For Non-uniform Fourier transformation (NUFFT), the online available Fessler toolbox has been used [18]. The objective function is the ℓ_1 norm that promotes sparsity. The constrained optimization problem in Eq. 1, was reformulated in an unconstrained optimization form by solving the Lagrangian ℓ_1-minimization problem:

Table 1 Acquisition time, percentage k-space filling, and effective number of averages for the different protocols

	FLASH fully sampled	UTE fully sampled	UTE 2×	UTE 4×	UTE 5×
Acquisition time	2 min 34 s	3 min 47 s	1 min	30 s	15 s
k-space filling[a]	95.7 ± 3.1 %	94.7 ± 4.1 %	55.6 ± 8.1 %	26.2 ± 5.6 %	19.9 ± 3.9 %
NA[a,b]	4.5 ± 0.3	3.4 ± 0.2	1.50 ± 0.09	1.16 ± 0.15	1.09 ± 0.11

[a] Values are mean ± standard deviation

[b] NA refers to the effective number of averages for the part of the k-space that was filled

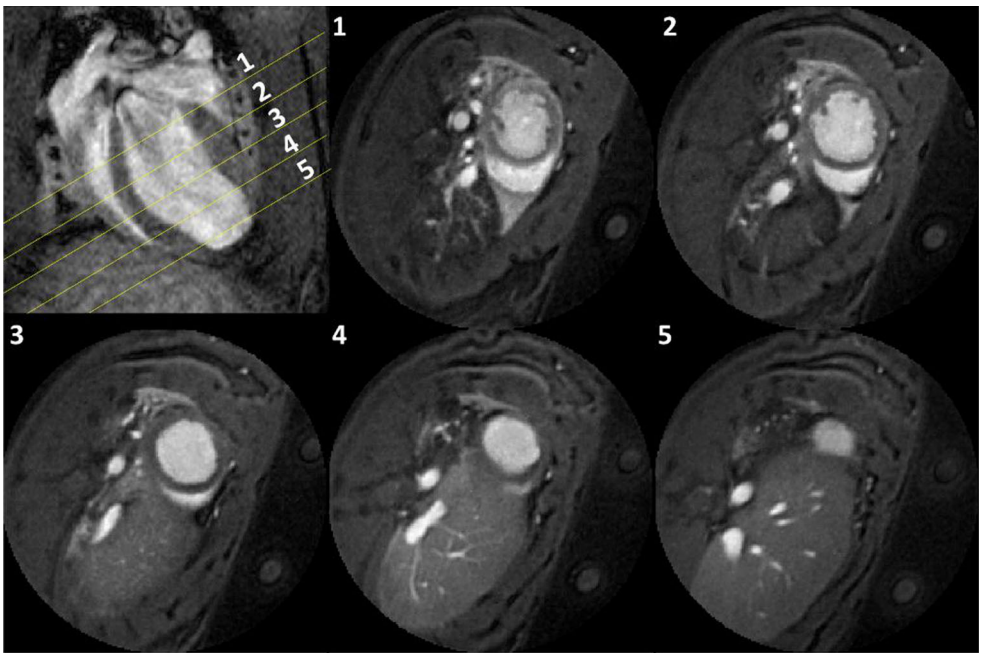

Fig. 2 Long-axis and 5 short-axis slices at end-diastole of an infarcted rat heart obtained with the fully sampled 3 min 47 s self-gated 2D UTE acquisition. The position of the 5 short-axis slices is indicated in the long-axis image

$$\min_{\mathrm{m}}\{||\mathrm{R}^{-1}\mathrm{F_s m}-\mathrm{y}||_2^2+\lambda||\Psi(\mathrm{m})||_1\} \quad (2)$$

where m is the Cine images to be reconstructed, λ is a weighting parameter, Ψ is the total-variation (TV) (sparse-transform) along the temporal direction defined as

$$\Psi(m)=|\beta_t(\mathrm{m})| \quad (3)$$

where m is a voxel, β_t is the finite difference in the temporal direction. The difference operator used for the total variation was a one-sided difference.

For successful compressed sensing application, sampling trajectories that induce incoherent, noise-like, artifacts should be used. This can be satisfied by using radial trajectories where undersampling is achieved in two dimensions. This makes radial sampling very robust with respect to undersampling, as the undersampling artifacts appear as slight streaking and increased pseudo-noise. In radial sampling, radial spokes passing through the k-space origin are acquired with uniform angular spacing. However, homogenous coverage and higher incoherence values were achieved by sampling with non-uniform golden-angle angular spacing [23–25]. This reduces the symmetry of the point spread function (PSF) of radial sampling, allowing for better compressed sensing reconstruction. The repetitive acquisition of the center of the k-space is of special interest, leading to dense oversampling of the center of k-space suppressing motion artifacts.

Self-gating

For self-gated cardiac Cine MRI, repeated acquisitions of specific region in k-space are performed to extract the cardiac and respiratory cycle information. For the FLASH sequence, self-gating information can be retrieved from the echo that is produced by the slice-refocusing gradient at the cost of increased TE [14]. In the radial acquisition scheme of the UTE sequence the center point in the k-space that is recorded each TR can be used for self-gating purposes. Cardiac triggering and respiratory gating is therefore derived directly from the radial readout with the shortest possible TE and TR.

Data analysis

To validate the multi-slice self-gated UTE reconstructions, cardiac functional parameters, i.e. end-systolic volume (ESV), end-diastolic volume (EDV), ejection fraction (EF), and cardiac output (CO), derived from the fully sampled and undersampled CS reconstructions were compared to those obtained from the FLASH acquisitions. Global heart parameters were derived using a semi-automatic segmentation with the QMass MR software (version 7.5) by Medis (Medis Medical Imaging Systems B.V., Leiden, The Netherlands). One person performed all the segmentations. Contours were manually corrected for the papillary muscle

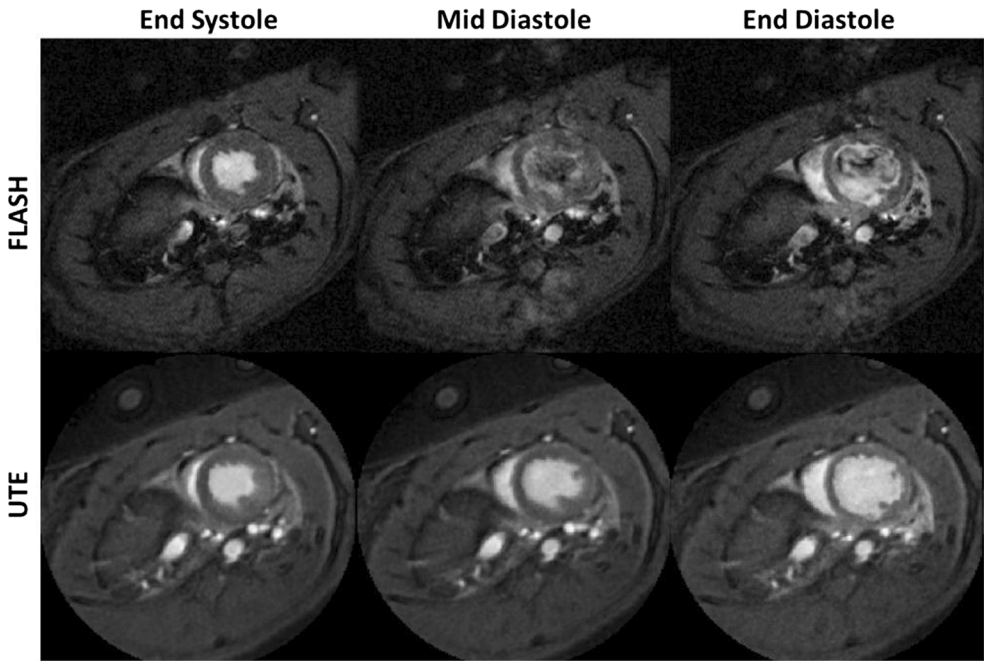

Fig. 3 Comparison of fully sampled FLASH and UTE. Short-axis mid-ventricular end-systolic, mid-diastolic, and end-diastolic time frames from a Cine of a healthy rat heart using the fully sampled self-gated FLASH and UTE scans. In contrast to the FLASH, the UTE scans are free from blood flow artifacts in the left and right ventricle

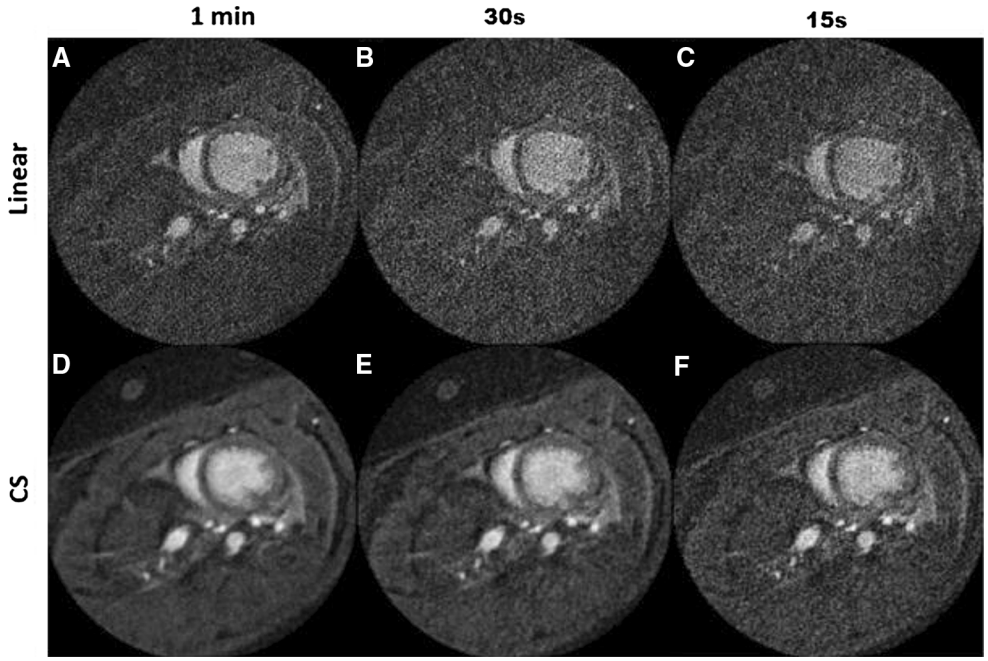

Fig. 4 Difference between linear and CS reconstructions of undersampled UTE scans. Shown is a mid-ventricular slice of a healthy rat heart and end-diastole. Image quality of linear reconstructions of the 2× (1 min), 4× (30 s), and 5× (15 s) undersampled data was poor with noise-like and streaking artifacts. The CS reconstruction mitigated the undersampling artifacts resulting in greatly improved image quality

area. Statistical analysis was performed using SPSS 20.0 (SPPS, Inc., Chicago, IL, USA). A *t* test with post hoc Bonferroni correction was performed to compare the EF for the different reconstructions between and within the healthy and infarct groups. The level of statistical significance was set at $p = 0.05$. A Bland–Altman analysis was

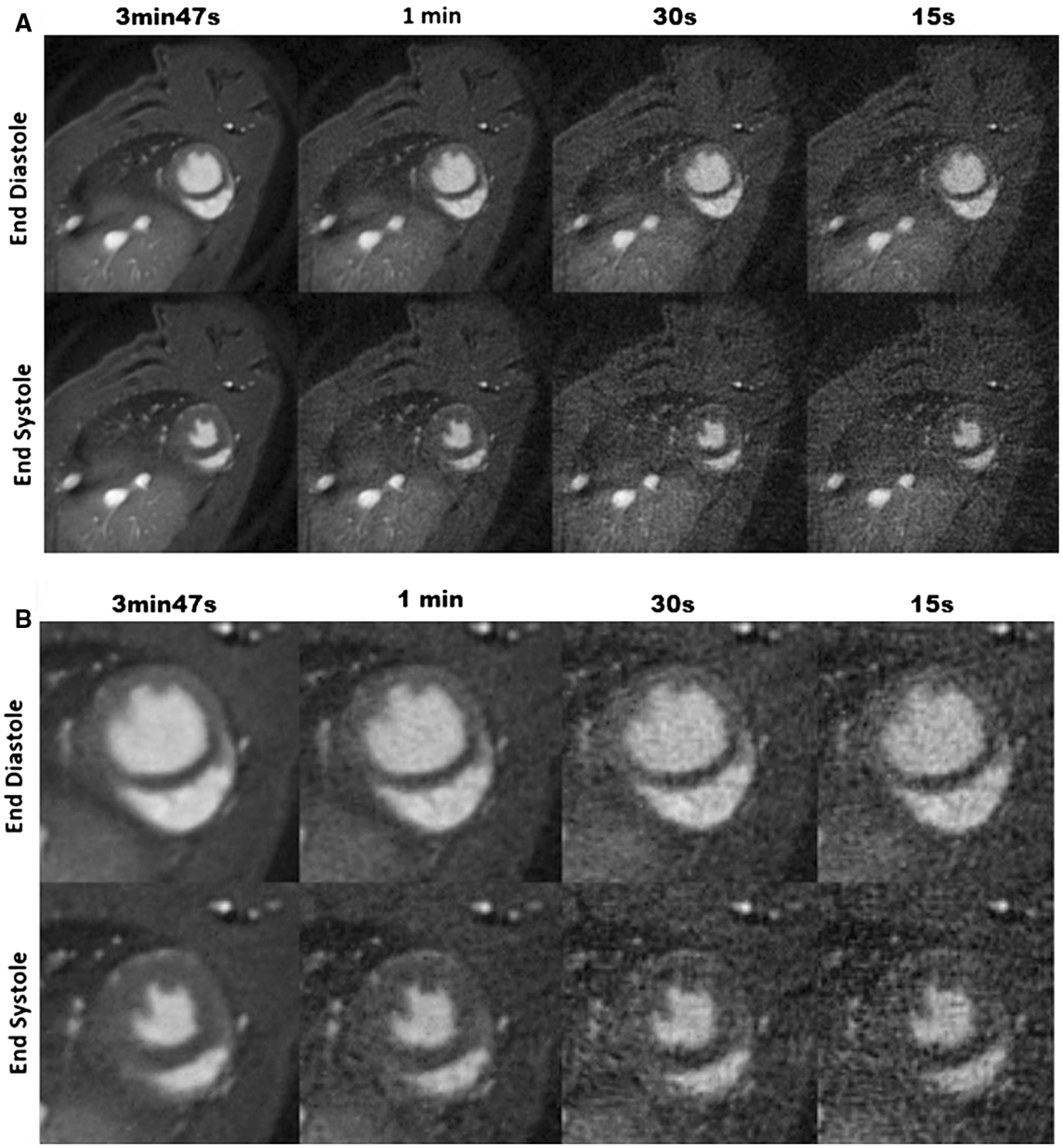

Fig. 5 Reconstructions of UTE scans of a healthy rat heart. **a** Short-axis frames at end-diastole and end-systole comparing the fully sampled UTE scan and the undersampled UTE scans with CS reconstruction. **b** Magnification of the region containing the heart

performed for ESV, EDV, EF, and CO to test the level of agreement between cardiac parameters derived from fully sampled and undersampled reconstructions.

Additionally, four independent observers, who were blinded to the type of sequence and reconstruction, visually scored the diagnostic quality of the movies from the different protocols. The movies were presented to the observers in a random order. Criteria included signal to noise (SNR), contrast to noise (CNR) between myocardium and blood pool, presence of reconstruction artifacts (e.g. streaking due to radial sampling or ghosting due to undersampling), and presence of flow artifacts. Scoring in these categories was performed on a standard 4 point scale, with 1 = poor to 4 = excellent for SNR and CNR, and 1 = uninterpretable due artifacts to 4 = no artifacts for scoring artifacts. A Wilcoxon's signed ranked test was used for comparing the scores. The level of statistical significance was set at $p = 0.05$.

Results

In Fig. 1a the 2D self-gated UTE sequence diagram is schematically drawn. The navigator information was

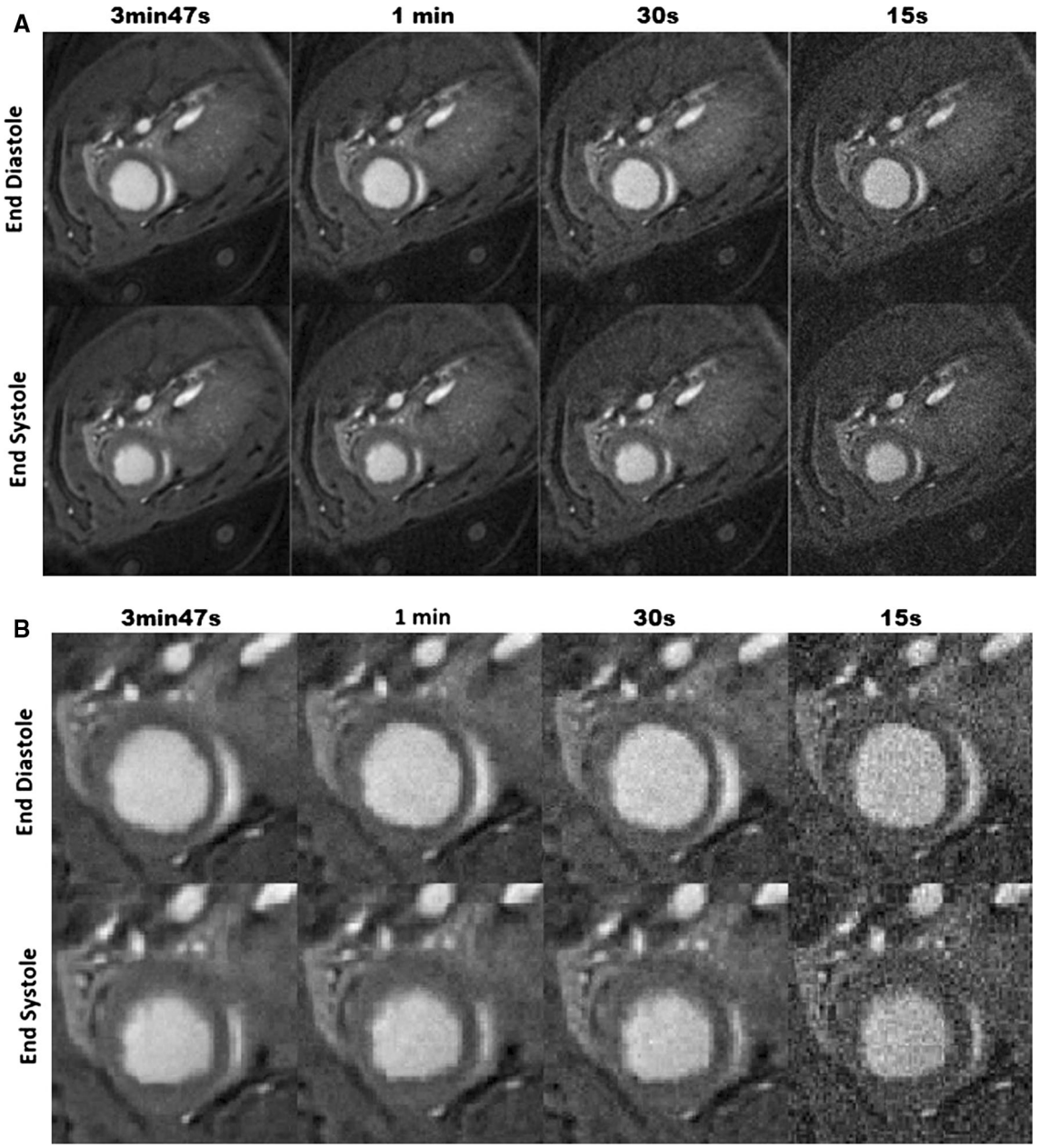

Fig. 6 Reconstructions of UTE scans of an infarcted rat heart. **a** Short-axis frames at end-diastole and end-systole comparing the fully sampled UTE scan and the undersampled UTE scans with CS reconstruction. **b** Magnification of the region containing the heart

obtained from the first sampled point at the start of the radial readout. Cardiac and respiratory cycles could be clearly distinguished in a trace of the navigator signal intensity, as shown in Fig. 1b for a representative example from one of the in vivo measurements. Consequently, the acquired radial k-lines could be accurately assigned to the corresponding cardiac time frames and approximately 30 % of the k-lines acquired during respiration were rejected. The average heart rate for all the rats included in the experiment was 348 ± 51 beats per min.

The top left panel in Fig. 2 shows a long-axis image of a rat with myocardial infarction at end-diastole with lines indicating the position of the 5 short-axis slices shown in the other panels. Long-axis and short-axis images were acquired with the fully sampled 3 min 47 s self-gated 2D UTE acquisition. The 5 slices covered the heart from base to apex. Good contrast between blood and myocardium was achieved, facilitating accurate segmentation of the left ventricular (LV) wall and lumen. Movies were visually free from flow or other artifacts.

Table 2 Average scoring of the different protocols by 4 observers

	FLASH fully sampled	UTE fully sampled	UTE 2×	UTE 4×	UTE 5×
SNR	3.13 ± 0.64	3.75 ± 0.44*	3.45 ± 0.52	2.87 ± 0.55$^{\#}$	2.66 ± 0.63$^{\#}$
CNR	3.52 ± 0.52	3.66 ± 058	3.56 ± 0.44	3.31 ± 0.54$^{\#}$	3.12 ± 0.66$^{\#}$
Reconstruction artifacts	3.33 ± 0.80	4.0*	3.64 ± 0.45*$^{\#}$	2.54 ± 0.50*$^{\#}$	2.12 ± 0.42*$^{\#}$
Flow artifacts	2.54 ± 0.46	4.0*	4.0*	4.0*	4.0*

Scoring in the categories SNR, CNR, presence of reconstruction artifacts, and presence of flow artifacts was performed on a standard 4-point scale, with 1 = poor to 4 = excellent for SNR and CNR, and 1 = uninterpretable due artifacts to 4 = no artifacts for scoring the presence of artifacts

All values are mean ± standard deviation

* Indicates significantly different from FLASH fully sampled

$^{\#}$ Indicates significantly different from UTE fully sampled

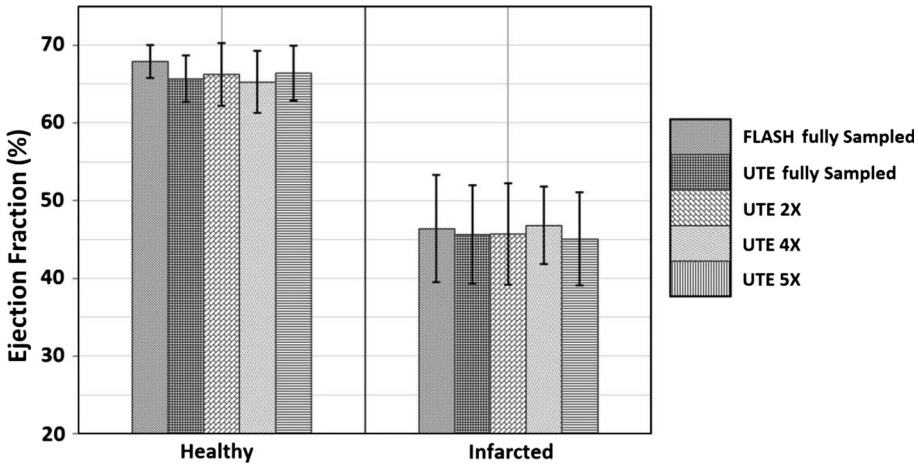

Fig. 7 Comparisons of EF between the experimental groups and for the FLASH and UTE acquisitions

A comparison between the fully sampled UTE Cine acquisition and the standard self-gated FLASH is presented in Fig. 3 for several time frames in the cardiac cycle at a mid-ventricular slice of a healthy rat. FLASH acquisitions suffered from flow artifacts particularly during the filling phases in diastole. In contrast, uniform blood signal intensity was observed in UTE acquisitions with no visible flow artifacts in the left and right ventricle.

Undersampling of the radial acquisition with golden-angle k-space filling leads to relatively mild artifacts using a standard linear Fourier transform reconstruction, as shown in the top row of Fig. 4 for the 1 min (2× undersampling), 30 s (4× undersampling) and 15 s (5× undersampling) at a mid-ventricular slice of a healthy rat at end-diastole. Undersamplng artifacts were incoherent and noise-like, which is a requirement facilitating CS reconstruction, clearly leading to improved image quality. Even for 5× undersampling in Fig. 4f the CS reconstruction nearly recovered the image quality of the 1 min linear reconstruction shown in Fig. 4a. Movies with higher undersampling factor were visually judged unfeasible for quantitative analysis.

Frames at end-diastole and end-systole, as well as magnifications of the heart region for fully sampled and undersampled UTE acquisitions are shown in Figs. 5 and 6 for a healthy rat and a rat with myocardial infarction, respectively. For all four healthy rats and the four rats with myocardial infarction, cardiac movies in all 5 slices were successfully reconstructed by CS up to 5× k*t*-space undersampling.

Four observers blinded to the type of scan and reconstruction method visually scored the quality of the cardiac movies using a standard 4-point scoring scale. The average scores in four categories, i.e. SNR, CNR between blood and myocardium, presence of reconstruction artifacts and presence of flow artifacts, are summarized in Table 2. As shown in the table, the quality of the fully sampled UTE movies was superior to the fully sampled FLASH movies. For the UTE protocols, there was a significant decrease in the average scoring of the SNR, CNR and reconstruction artifacts with increasing degree of undersampling. In contrast to the FLASH protocol, the UTE protocols were free of flow-artifact free images.

For a quantitative analysis, in Fig. 7 a bar chart of the EF for the healthy and infarct rats comparing FLASH and

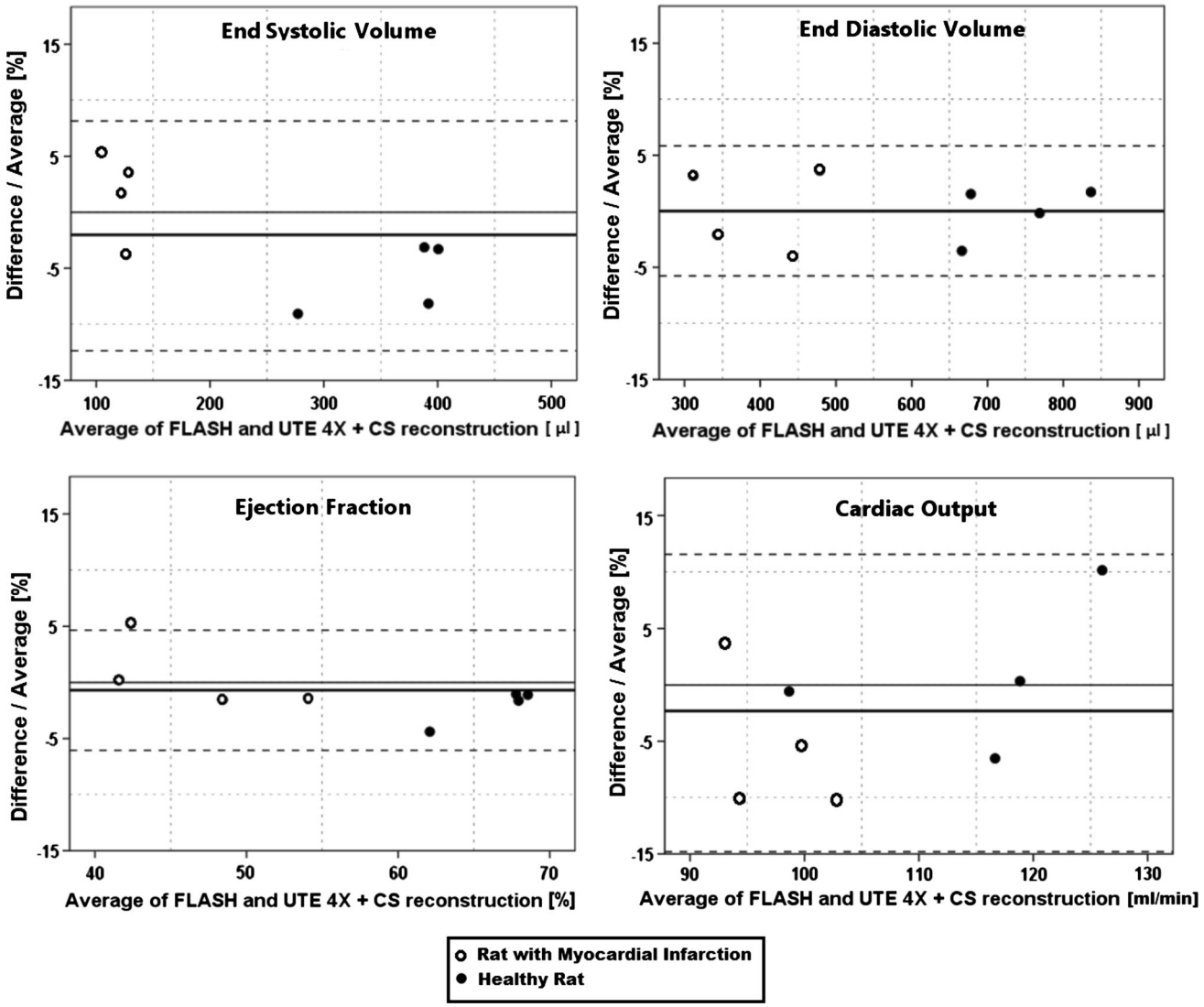

Fig. 8 Bland–Altman analysis of the heart functional parameters for 4× undersampled UTE in comparison to fully sampled FLASH. Solid and open points indicate data for healthy and infarcted rat hearts, respectively

Table 3 Bland–Altman analysis of cardiac functional parameters

	UTE fully sampled	UTE 2×	UTE 4×	UTE 5×
ESV	−0.2 ± 11.0	−2.1 ± 10.5	−2.1 ± 10.3	−4.1 ± 9.5
EDV	−0.5 ± 4.3	−0.1 ± 5.2	0.04 ± 5.80	−0.0 ± 5.6
EF	−1.6 ± 2.8	−1.0 ± 2.6	−0.7 ± 5.4	−1.2 ± 2.4
CO	−3.7 ± 7.1	−3.1 ± 6.0	−2.3 ± 13.9	−4.2 ± 8.3

Comparisons of FLASH with UTE protocols

All values are mean ± 1.96 standard deviation in percentages

ESV end-systolic volume, *EDV* end-diastolic volume, *EF* ejection fraction, *CO* cardiac output

UTE acquisitions is shown. As expected, the animals with myocardial infarction showed significantly lower EF ($p < 0.05$) than healthy ones in both FLASH and UTE images. Within the standard deviation of the admittedly limited (N = 4) number of animals there were no statistical differences between FLASH, fully sampled, and accelerated UTE acquisitions within the infarct and healthy groups.

Additionally, to evaluate the effect of CS reconstruction and degree of undersampling on derived heart functional parameters of standard and CS reconstructions in more detail, ESV, EDV, EF, and CO from the FLASH and UTE scans were compared. As an example, Fig. 8 shows the Bland–Altman plot for the functional parameters of a 4× undersampled UTE acquisition with CS reconstruction compared to the FLASH acquisition for the 8 rats included in the experiment. Differences in ESV, EDV, EF and CO only had a small bias. Table 3 summarizes the Bland–Altman analysis of the heart functional parameters for all the UTE acquisitions compared to the FLASH scans.

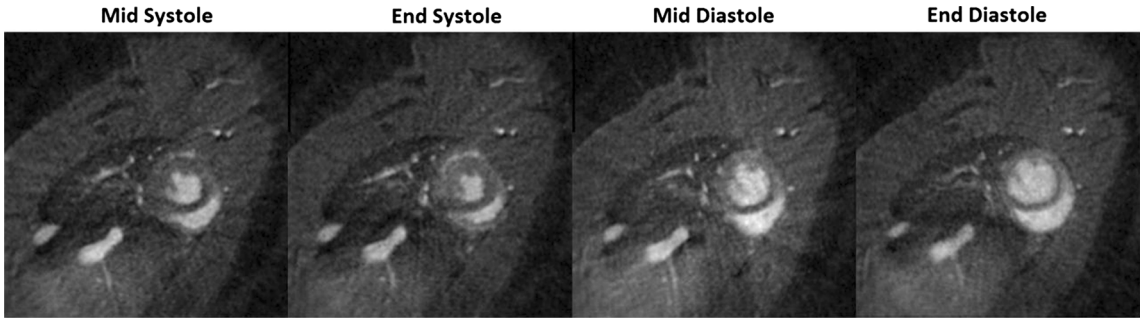

Fig. 9 High frame rate CINE UTE reconstruction. Short-axis slices of a healthy rat heart at various time points in the cardiac cycle taken from a 60-frames CINE. The data was recorded using the self-gated UTE with a total acquisition time of 1 min and 5× undersampling

Discussion

Radial k-space encoding schemes are becoming popular and find successful applications in clinical and preclinical studies [26–28]. The repetitive and dense acquisition of the center of the k-space makes the sequence relatively robust to motion [29]. This allows for better performance in capturing dynamic information. Besides, radial undersampling results in relatively mild streaking artifacts, which can be effectively removed by novel compressed sensing reconstruction methods making the technique suitable for high acceleration factors [23, 24].

The short TE that can be achieved in UTE sequences traditionally finds applications in bone, fibro-cartilage and lung imaging [30, 31]. Radial and spiral k-space filling schemes are employed for cardiovascular imaging in humans [27, 32–36] and animals [28, 37–40]. Recently, UTE MRI was employed to detect developing myocardial fibrosis after myocardium infarction, exploiting the short T_2 of fibrous tissue [37, 38]. Moreover, a radial readout proved beneficial in phase-contrast velocity encoded imaging for high velocity blood flow quantification in stenotic jets, present in arterial occlusions due to atherosclerosis, which cannot be recorded using the conventional phase contrast sequences with longer TE [41].

In this study, an accelerated 2D multi-slice self-gated UTE sequence was implemented. Ultimately, volumetric imaging with 3D radial readout would be even more favorable. In 3D, the undersampling artifacts display more incoherence, which allows for a higher degree of acquisition undersampling [17, 23]. Moreover, in our sequence TE could be further reduced from 290 μs for 2D to about 20–50 μs for 3D due to the absence of a slice selection refocusing gradient.

Presently, for the 15-frame Cine reconstructions 5× undersampling was the upper limit. With this technology the measurement of a single slice takes only 15 s and full heart coverage was obtained within 1 min 30 s, which is much faster than traditional murine Cine imaging [14, 15]. For higher undersampling factors a number of frames within the cardiac cycle displayed artifacts that made them unsuitable for accurate segmentation and further analysis. The number of frames with artifacts increased with acceleration factor.

Qualitative visual scoring of movie quality by four blinded observers revealed that quality of the fully sampled UTE movies was superior to the fully sampled FLASH movies, primarily due to the absence of flow artifacts in the UTE protocols. For the UTE protocol, SNR and CNR decreased with increasing degree of undersampling and the number of reconstruction artifacts increased. Nevertheless, a quantitative comparison revealed no statistical difference between the mean EF derived from movies obtained by the different protocols (Fig. 7) and Bland–Altman analysis (Fig. 8) showed only minor differences for the cardiac functional parameters ESV, EDV, EF, and CO of FLASH and UTE protocols. Taken together, this shows that LV functional parameters could be derived accurately with the UTE protocol and CS reconstruction up to 5× undersampling.

Since we are using a self-gated sequence with no ECG triggering, filling of k*t*-space cannot be fully predetermined as it relies on the asynchronous timing between heartbeat, respiration and TR. The effective number of averages for the acquired k-lines and the percentage of k-space filling therefore vary over the acquisitions (Table 1) as well as over the cardiac time frames. The acquisition of a fully sampled dataset therefore takes relatively long as we have to ensure that at least approximately 95 % of all k-lines are filled [15, 42].

The use of self-gating has the distinct advantage that the number of time frames in the cardiac cycle is not predetermined but can be chosen after scan completion. In this work, the standard Cine reconstructions were performed with 15 cardiac time frames. However, we can also achieve a higher number of cardiac frames with the same effective undersampling factor at the expense of a longer acquisition time. High frame rate Cine is useful to assess diastolic

function, which requires a high temporal resolution particularly in the filling phase of the heart [15, 42]. As an example, in Fig. 9 several frames from a 60-frame Cine are shown, reconstructed from a 1 min acquisition with 5× undersampling.

In this paper, we implemented a self-gated UTE sequence with golden-angle radial acquisition and CS reconstruction for studying murine heart. We believe that self-gating and accelerated UTE scanning could also prove beneficial for human application to decrease scanning time and reduce image artifacts, particularly at high magnetic field strengths.

Conclusions

In summary, in this work we presented a multi-slice UTE MRI protocol for whole heart Cine imaging of the rat heart. The technique exploits the self-gated acquisition scheme to produce an undersampled, random k*t*-space. CS reconstructions were successful in mitigating undersampling artifacts up to 5× undersampling. Whole heart coverage 15-frame Cine was achieved in 1min30 s. Cardiac functional parameters of healthy and infarcted rat hearts derived from fully and undersampled acquisitions were statistically the same as those derived from standard Cine FLASH.

Acknowledgments We thank Leonie Niesen for biotechnical assistance.

Conflict of interest None.

References

1. McVeigh ER (1998) Regional myocardial function. Cardiol Clin 16:189–206
2. Watzinger N, Saeed M, Wendland MF, Akbari H, Lund G, Higgins CB (2001) Myocardial viability: magnetic resonance assessment of functional reserve and tissue characterization. J Cardiovasc Magn Reson 3:195–208
3. Kim RJ, Wu E, Rafael A, Chen E, Parker MA, Simonetti O, Klocke FJ, Bonow RO, Judd RM (2000) The use of contrast-enhanced magnetic resonance imaging to identify reversible myocardial dysfunction. N Engl J Med 343:1445–1453
4. Geelen T, Paulis LEM, Coolen BF, Nicolay K, Strijkers GJ (2012) Contrast-enhanced MRI of murine myocardial infarction—part I. NMR Biomed 25:953–968
5. Kober F, Bernard M, Troalen T, Capron T (2012) Cardiovascular magnetic resonance of myocardial structure, function, and perfusion in mouse and rat models. Curr Cardiovasc Imag Rep 5:109–115
6. Shin T, Hu HH, Pohost GM, Nayak KS (2008) Three dimensional first-pass myocardial perfusion imaging at 3T: feasibility study. J Cardiovasc Magn Reson 10:57
7. Peters DC, Korosec FR, Grist TM, Block WF, Holden JE, Vigen KK, Mistretta CA (2000) Undersampled projection reconstruction applied to MR angiography. Magn Reson Med 43:91–101
8. Thedens D, Irarrazaval P, Sachs T, Meyer C, Nishimura D (1999) Fast magnetic resonance coronary angiography with a three-dimensional stack of spirals trajectory. Magn Reson Med 41:1170–1179
9. Frahm J, Haase A, Matthaei D (1986) Rapid NMR imaging of dynamic processes using the FLASH technique. Magn Reson Med 3:321–327
10. Robson MD, Gatehouse PD, Bydder M, Bydder GM (2003) Magnetic resonance: an introduction to ultrashort TE (UTE) imaging. J Comput Assist Tomogr 27:825–846
11. O'Brien KR, Gabriel RS, Greiser A, Cowan BR, Young AA, Kerr AJ (2009) Aortic valve stenotic area calculation from phase contrast cardiovascular magnetic resonance: the importance of short echo time. J Cardiovasc Magn Reson 11:49–60
12. Hoerr V, Nagelmann N, Nauerth A, Kuhlmann M, Stypmann J, Faber C (2013) Assessment of functional cardiac parameters at high magnetic fields. J Cardiovasc Magn Reson 15:59
13. Heijman E, Graaf WD, Niessen P, Nauerth A, Eys G, Graaf LD, Nicolay K, Strijkers GJ (2007) Comparison between prospective and retrospective triggering for mouse cardiac MRI. NMR Biomed 20:439–447
14. Nauerth A, Heijman E, Diekmann C (2006) Slice refocusing signal for retrospective reconstruction of CINE cardiac MR images. Proc Intl Soc Magn Reson Med 14, p 1648
15. Coolen BF, Abdurrachim D, Motaal AG, Nicolay K, Prompers JJ, Strijkers GJ (2013) High frame rate retrospectively triggered Cine MRI for assessment of murine diastolic function. Magn Reson Med 69:648–656
16. Larson A, White R, Laub G, McVeigh E, Li D, Simonetti O (2004) Self-gated cardiac cine MRI. Magn Reson Med 51:93–102
17. Lustig M, Donoho D, Pauly JM (2007) Sparse MRI: the application of compressed sensing for rapid MR imaging. Magn Reson Med 58:1182–1195
18. Fessler JA, Sutton BP (2003) Nonuniform fast fourier transforms using min–max interpolation. IEEE Trans Signal Process 51(2):560–574
19. Wech T, Lemke A, Medway D, Stork L-A, Lygate CA, Neubauer S, Kostler H, Schneider JE (2011) Accelerating cine-MR imaging in mouse hearts using compressed sensing. J Magn Reson Imag 34:1072–1079
20. Otazo R, Kim D, Axel L, Sodickson DK (2010) Combination of compressed sensing and parallel imaging for highly accelerated first-pass cardiac perfusion MRI. Magn Reson Med 64:767–776
21. Gamper U, Boesiger P, Kozerke S (2008) Compressed sensing in dynamic MRI. Magn Reson Med 59:365–373
22. Buonincontri G, Methner C, Krieg T, Carpenter TA, Sawiak SJ (2014) Functional assessment of the mouse heart by MRI with a 1-min acquisition. NMR Biomed 27:733–737
23. Doneva M, Eggers H, Rahmer J, Börnert P, Mertins A (2008) Highly undersampled 3D golden ratio radial imaging with iterative reconstruction. Proceedings of the 16th annual meeting of ISMRM, Toronto, Canada, p 336
24. Feng L, Grimm R, Block KT, Chandarana H, Kim S, Xu J, Axel L, Sodickson DK, Otazo R (2014) Golden-angle radial sparse parallel MRI: combination of compressed sensing, parallel imaging, and golden-angle radial sampling for fast and flexible dynamic volumetric MRI. Magn Reson Med. doi:10.1002/mrm.24980
25. Winkelmann S, Schaeffter T, Koehler T, Eggers H, Doessel O (2007) An optimal radial profile order based on the golden ratio for time-resolved MRI. IEEE Trans Med Img 26:68–76
26. Thompson RB, McVeigh ER (2004) Flow-gated phase-contrast MRI using radial acquisitions. Magn Reson Med 52:598–604
27. Bauer RW, Radtke I, Block KT, Larson MC, Kerl JM, Hammerstingl R, Graf TG, Vogl TJ, Zhang S (2013) True real-time cardiac MRI in free breathing without ECG synchronization using a novel sequence with radial k-space sampling and balanced SSFP contrast mode. Int J Cardiovasc Imag 29(5):1059–1067

28. Hiba B, Richard N, Thibault H, Janier M (2007) Cardiac and respiratory self-gated cine MRI in the mouse: comparison between radial and rectilinear techniques at 7T. Magn Reson Med 58(4):745–753
29. Glover GH, Pauly JM (1992) Projection reconstruction techniques for reduction of motion effects in MRI. Magn Reson Med 28:275–289
30. Bergin CJ, Glover GH, Pauly JM (1991) Lung parenchyma: magnetic susceptibility in MR imaging. Radiology 180:845–848
31. Du JA, Carlb M, Byddera M, Takahashib A, Chunga CB, Byddera GM (2010) Qualitative and quantitative ultrashort echo time (UTE) imaging of cortical bone. J Magn Reson 207:304–311
32. Krämer M, Herrmann K-H, Biermann J, Reichenbach JR (2014) Retrospective reconstruction of cardiac cine images from golden-ratio radial MRI using one-dimensional navigators. J Magn Reson Imag. doi:10.1002/jmri.24364
33. Jung H, Park J, Yoo J, Ye JC (2010) Radial k-t FOCUSS for high-resolution cardiac cine MRI. Magn Reson Med 63:68–78
34. Bauer R, Radtke I, Uecker M, Zhang S, Block K, Graf T, Kerl J, Vogl T, Larson M True real-time cardiac MRI with radial K-space sampling in free breathing without ECG-synchronization—improved image quality with iterative image reconstruction. Radiological Society of North America 2012 Scientific Assembly and Annual Meeting; 2012 Chicago, IL
35. Seiberlich N, Lee G, Ehses P, Duerk JL, Gilkeson R, Griswold M (2011) Improved temporal resolution in cardiac imaging using through-time spiral GRAPPA. Magn Reson Med 66:1682–1688
36. Usman M, Atkinson D, Odille F, Kolbitsch C, Vaillant G, Schaeffter T, Batchelor P, Prieto C (2013) Motion corrected compressed sensing for free-breathing dynamic cardiac MRI. Magn Reson Med 70:504–516
37. Jong SD, Zwanenburg JJ, Visser F, Nagel RVD, Rijen HV, Vos MA, Bakker JM, Luijten PR (2011)Direct detection of myocardial fibrosis by MRI. J Mol Cell Cardiol 51(6):974–979
38. Nierop BV, Nelissen JL, Bax NA, Graaf L, Nicolay K, Strijkers GJ In vivo ultra short TE (UTE) MRI of mouse myocardial infarction. In: Proceedings of the 20th annual meeting of ISMRM, Melbourne, Australia, p 390
39. Hiba B, Richard N, Janier M, Croisille P (2006) Cardiac and respiratory double self-gated cine MRI in the mouse at 7 T. Magn Reson Med 55:506–513
40. Voiron J, Lamalle L (2006) Spiral MRI on rat brain and rat heart at 7 Tesla. In: Proceedings of the 14th annual meeting of ISMRM, Seattle, Washington, USA, p 3378
41. O'Brien KR,Myerson SG,Cowan BR, Young AA, Robson MD (2009) Phase contrast ultrashort TE: a more reliable technique for measurement of high-velocity turbulent stenotic jets. Magn Reson Med 62(3):626–636
42. Motaal AG, Coolen BF, Abdurrachim D, Castro RM, Prompers JJ, Florack LM, Nicolay K, Strijkers GJ (2012) Accelerated high-frame-rate mouse heart cine-MRI using compressed sensing reconstruction. NMR Biomed 26(4):451–457